Research in Astron. Astrophys. **2009** Vol. **9** No. **6**, 665 – 681
http://www.raa-journal.org *http://www.iop.org/journals/raa*

***R**esearch in*
***A**stronomy and*
***A**strophysics*

Ionization state of cosmic hydrogen by early stars and quasars

Xiao-Chun Mao[1,2]

[1] National Astronomical Observatories, Chinese Academy of Sciences, Beijing 100012, China; *xcmao@bao.ac.cn*
[2] Graduate University of Chinese Academy of Sciences, Beijing 100049, China

Received 2008 September 8; accepted 2008 December 14

Abstract Cosmic hydrogen is reionized and maintained in its highly ionized state by the ultraviolet emission attributed to an early generation of stars and quasars. The Lyα opacity observed in absorption spectra of high-redshift quasars permits more stringent constraints on the ionization state of cosmic hydrogen. Based on density perturbation and structure formation theory, we develop an analytic model to trace the evolution of the ionization state in the post-overlap epoch of reionization, in which the bias factor is taken into account. For quasars, we represent an improved luminosity function by utilizing a hybrid approach for the halo formation rate that is in reasonable agreement with the published measurements at $2 \lesssim z \lesssim 6$. Comparison with the classic Press-Schechter mass function of dark matter halos, we demonstrate that the biased mass distribution indeed enhances star formation efficiency in the overdense environment by more than 25 per cent following the overlap of ionized bubbles. In addition, an alternative way is introduced to derive robust estimates of the mean free path for ionizing photons. In our model, star-forming galaxies are likely to dominate the ionizing background radiation beyond $z = 3$, and quasars contribute equally above a redshift of $z \sim 2.5$. From $5 \leqslant z \leqslant 6$, the lack of evolution in photoionization rate can thus be explained by the relatively flat evolution in star formation efficiency, although the mean free path of ionizing photons increases rapidly. Moreover, in the redshift interval $z \sim 2 - 6$, the expected mean free path and Gunn-Peterson optical depth obviously evolve by a factor of ~ 500 and ~ 50 respectively. We find that the relative values of critical overdensities for hydrogen ionization and collapse could be 430% at $z \approx 2$ and 2% at $z \approx 6$, suggesting a rapid overlap process in the overdense regions around instant quasars following reionization. We further illustrate that the absolute estimates of the fraction of neutral hydrogen computed from theoretical models may not be important because of comparable uncertainties in the computation.

Key words: cosmology: theory — formation: galaxies — quasars: general — diffuse radiation — intergalactic medium

1 INTRODUCTION

Reionization of cosmic hydrogen provides unique insight into the early history of structure formation. The recent observations of the Lyα opacity distribution in high-redshift quasar spectra have allowed more reliable analysis of the properties of ionizing sources as well as the intergalactic medium (IGM). The appearance of these Lyman series absorption lines indicates that the reionization of cosmic hydrogen was completed around $z = 6$ with a volume weighted neutral fraction of

$\langle f_{\rm HI}\rangle_{\rm V} \sim 10^{-3.5}$ (e.g. White et al. 2003; Fan et al. 2006; Becker et al. 2007), and just above $z \sim 6$, the existence of the Gunn-Peterson trough (Gunn & Peterson 1965) at wavelengths blueward of the Lyα emission line suggests that a significant fraction of neutral hydrogen ($\gtrsim 1$ in mass average Becker et al. 2001; Djorgovski et al. 2001; Fan et al. 2002). Under the assumptions for the quasar age and ionizing luminosity, the observed HII region sizes surrounding high-redshift quasars could also provide a powerful and independent way to measure the neutral hydrogen fraction in the IGM (see Wyithe et al. 2005; Mesinger & Haiman 2007; Bolton & Haehnelt 2007a). Additionally, with a large set of detailed radiative transfer simulations, Bolton & Haehnelt (2007b) have assessed the potential of the ratio of Lyβ to Lyα near-zone sizes as a probe of the HI fraction at $z > 6$. They found that a future sample of several tens of high resolution quasar spectra would be required to distinguish the IGM which has an HI fraction greater or lower than 10 per cent at the 3σ level.

On the other hand, a great amount of literature has claimed that examining the nature and evolution of the ionization state of cosmic hydrogen by interpreting the observed absorption spectra of high-redshift QSOs is really complicated and problematic, especially at redshifts approaching and beyond the tail-end of the reionization epoch at $z \approx 6$. Maselli et al. (2007), see also Bolton & Haehnelt (2007a) and Lidz et al. (2007), have investigated that the small transmission regions in quasar spectra can be understood as either HII ionization fronts or classical proximity zones due to enhanced ionizing flux near the quasars (Bajtlik et al. 1988). Moreover, the ambiguity in distinguishing the edge of ionized regions and the insufficient sample of instant quasars both make it difficult to place stronger constraints on the reionization process at high redshifts. For the Lyman series absorption, the main limitation is that it becomes completely saturated as the neutral hydrogen fraction reaches $\langle f_{\rm HI}\rangle_{\rm V} > 10^{-3}$, owing to the large cross-section of the Lyα resonance associated with the considerable systematic observational errors in the red and near-IR part of these spectra (Fan et al. 2006; Bolton & Haehnelt 2007a; Wyithe 2008). Combined with the radiative transfer and feedback effects, large scatter in the UV flux along different lines-of-sight further complicates the physical picture. In addition, the parameters adopted in previous studies, such as the escape fraction of ionizing photons $f_{\rm esc}$, the quasar age and luminosity, have great uncertainties. In most previous investigations of the reionization process, the QSOs and galaxies are implicitly assumed to be located in cosmic average regions (Yu & Lu 2005). However, in the hierarchical formation and evolution scenario of QSOs and galaxies (e.g. Kauffmann & Haehnelt 2000), luminous QSOs are embedded in a rare overdense environment. The underlying fluctuations in this density field would introduce some obvious variations in the inferred ionizing continuum that significantly deviates from the cosmic mean distribution over a wide range of redshifts (e.g. Yu & Lu 2005; Becker et al. 2007; Bolton & Haehnelt 2007b). Some discussions in a few recent papers are also related to the biasing effects (e.g, Cen 2003; Wyithe et al. 2007).

However, it is generally agreed that the first stars and high-redshift quasars dominate the emission of ionizing photons, and they contribute almost equally at $z \sim 2-3$ (e.g. Barkana & Loeb 2001; Kriss et al. 2001; Smette et al. 2002; Srbinovsky & Wyithe 2007). Furthermore, this photon budget just struggles to be sufficient to reionize the cosmic hydrogen and keep the highly ionized state by $z \sim 6$ (e.g. Lehnert & Bremer 2003; Schirber & Bullock 2003; Dijkstra et al. 2004; Gnedin et al. 2007; Shankar & Mathur 2007). In fact, the prediction for the ionization state depends strongly on the photoionization model and the IGM density profile. Gunn & Peterson (1965) first noted that even a neutral hydrogen fraction $\sim 10^{-5}$ is sufficient for gas to absorb photons strongly at the Lyα resonance. Thus, the pattern of density distribution around host halos may affect the observable properties of Lyα absorption although the density field decreases rapidly out to the virial radius of halos. Taking this density dependence into account, Loeb & Eisenstein (1995) explored the proximity effect and argued that neglecting the enhanced densities due to gas infall can lead to an overestimate of the ionizing flux by up to a factor of 3. In addition, Bolton & Haehnelt (2007c) have probed the ionizing emissivity at $z \geq 5$, and further suggested an extended photon-starved epoch of reionization. Nevertheless, one should keep it in mind that an extra population of ionizing sources, such as mini-quasars with harder spectra and the undetected dwarf galaxies, is also able to generate the missing UV emission during reionization (Dijkstra et al. 2004; Wyithe & Loeb 2006).

In this work, we present a theoretically derived and density dependent model to probe the ionization state of cosmic hydrogen at the post-overlap era of reionization. Based on the fact that the ionizing sources are located in the rare overdense environment, we employ $\bar{\delta}_R$ to describe the density distribution of the IGM in these highly biased regions, and further develop the quasar luminosity function and explore the redshift dependence of the mean free path for ionizing photons. Our related estimates of the photoionization rate, the Lyα effective optical depth and the neutral hydrogen fraction are then contrasted with the recent measurements of the Lyα opacity in quasar absorption spectra (e.g. Tytler et al. 2004; Kirkman et al. 2005; Fan et al. 2006; Shapley et al. 2006), combined with a large suite of high-resolution hydrodynamical simulations (e.g. McDonald & Miralda-Escudé 2001; Bolton et al. 2005; Bolton & Haehnelt 2007c). Comparison of the ionization state inferred from the physically motivated model with the direct observations would improve our ability to understand the reionization history and the IGM properties.

We begin by introducing the analytic reionization model in Section 2. The procedure for examining the Lyman limit flux contributed by both galaxies and quasars is presented carefully. Uncertainties in the model parameters are also discussed here. In Section 3, we first pay particular attention to the evolution of the mean free path, and then connect it to the photoionization rate and the GP optical depth in the redshift interval $2 \lesssim z \lesssim 6$. We further analyze the plausible evolutionary trend of the neutral hydrogen fraction over the same redshift range in detail. Meanwhile, the results derived from our model are compared with measurements and simulations. Lastly, we conclude with a discussion in Section 4. Throughout the paper, we adopt a concordance cosmology of $\Omega_0 = 0.265$, $\Omega_\Lambda = 0.735$, $\Omega_{\rm b} = 0.044$, $h = 0.71$, $n_{\rm s} = 1$ and $\sigma_8 = 0.772$, as revealed by the WMAP three-year observations (Spergel et al. 2007).

2 ANALYTIC MODEL FOR REIONIZATION

In this section, we develop an analytic model to quantify the ionizing background radiation emitted by the first stars and quasars respectively. Firstly, the physical basis for the formation of cosmic structure in initial overdense regions is reviewed in Section 2.1. Based on this, we present an improved description for the quasar luminosity function, and turn it into quasar ionizing intensity in Section 2.2. Subsequently, the star formation efficiency $f_\star(z)$ is formulated by a hybrid mass function of dark matter halos. Associated with the escape fraction of ionizing photons, we then convert $f_\star(z)$ to the stellar ionizing emissivity and directly evaluate the corresponding UV flux at the Lyman limit. In our calculation, the intensity absorption due to residual neutral hydrogen is examined by different considerations for galaxies and quasars. We then discuss how the reionization process depends on our model parameters in Section 2.4.

2.1 Density Fluctuations in Overdense Environment

The typical density profile around initial overdensities is directly related to the star formation history and the resonant Lyα absorption observed in quasar spectra. To describe the inhomogeneity of the density distribution, let us define the mean overdensity within a sphere with comoving radius R at redshift z: $\bar{\delta}_R \equiv [\langle\rho\rangle_R - \bar{\rho}]/\bar{\rho}$, in which $\langle\rho\rangle_R$ and $\bar{\rho}$ are the comoving average mass density in the sphere and the comoving cosmic mean mass density, respectively. Within virialized dark matter halos, the cosmic spherically-averaged density profile has been roughly described by Navarro, Frenk & White (1997) using numerical simulations of hierarchical halo formation. Barkana (2004) developed an analytic model for gas infall that is applicable to the average density profile outside the virial radius. Meanwhile, we adopt the definition that halos of a given mass form as long as their overdensities averaged on a scale exceed the critical threshold for collapse (e.g. Press-Schechter 1974; Loeb & Eisenstein 1995). The value of the threshold δ_c is determined utilizing the spherical collapse model and depends on the cosmological parameters (Peebles 1980; Eke et al. 1996; Barkana 2004). A realistic prescription has been provided by the various literature cited above. In what follows, we directly employ the expression of the average overdensity around virialized halos of mass M and refer the reader to the original papers for

more details.

$$\frac{\bar{\delta}_{\rm R}(M,R,z)}{\delta_{\rm c}} = 1-\Big(1-\alpha+\frac{\alpha}{\beta}\Big)\,{\rm erf}\Bigg[\sqrt{\frac{\beta(1-\alpha)}{2\alpha}}\Bigg] -\sqrt{\frac{2\alpha(1-\alpha)}{\pi\beta}}\,\exp\Big[-\frac{\beta(1-\alpha)}{2\alpha}\Big], \quad (1)$$

where we define

$$\alpha\equiv\frac{\xi_{\rm R}(R_{\rm M},R)}{\sigma^2(R_{\rm M},z)};\qquad \beta\equiv\frac{\delta_{\rm c}^2\alpha(1-\alpha)}{\sigma^2(R,z)-\alpha\xi_{\rm R}(R_{\rm M},R)}. \quad (2)$$

In linear theory, $\sigma^2(R,z)=D^2(z)\int_0^\infty\frac{dk}{2\pi^2}k^2P(k)W^2(kR)$ is the variance of the density fluctuations at redshift z within comoving radius R, and $\xi_{\rm R}(R_{\rm M},R)\equiv\int_0^\infty\frac{dk}{2\pi^2}k^2P(k)W(kR_{\rm M})W(kR)$ is the cross-correlation in which $R_{\rm M}=(3M/4\pi\bar{\rho})^{1/3}$. Hereafter, $P(k)$ and $W(kR)$ represent the initial matter power spectrum and the spherical top-hat window function, respectively.

Next, we concentrate on the mass distribution of dark matter halos formed in the biased regions. It has been pointed out that the classic Press-Schechter mass function (1974) fits high-resolution simulations only roughly, particularly at high mass-scales, and around the exponential turn-off (e.g. Hernquist & Springel 2003; Barkana & Loeb 2004; Yu & Lu 2005). To generalize the PS model, Sheth & Tormen (1999) added two free parameters with which the formula has been proved to match the numerical simulations more accurately (Jenkins et al. 2001) and allows for ellipsoidal collapse.

$$f_{\rm ST}[\delta_{\rm c},\sigma^2(R_{\rm M},z)] = \frac{A'}{\sqrt{2\pi}}\frac{\sqrt{a'}\nu}{\sigma^2(R_{\rm M},z)}\Big[1+\frac{1}{(a'\nu^2)^{q'}}\Big]\exp\Big(-\frac{a'\nu^2}{2}\Big) \quad (3)$$

with the best-fit parameters $a'=0.707$, $q'=0.3$ and the normalization parameter $A'=0.322$ (Sheth & Tormen 2002). Here ν is defined as $\nu\equiv\delta_c/\sigma(R_{\rm M},z)$. However, as usually argued, the halo mass function in the overdense environment would strongly deviate from the cosmic mean distribution. Then, within the extended Press-Schechter theory (Bond et al. 1991; Lacey & Cole 1993), the biased halo mass function in a region with average overdensity $\bar{\delta}_{\rm R}$ can be given by

$$f_{\rm bias-PS}[\delta_{\rm c},\sigma^2(R_{\rm M},z);\bar{\delta}_{\rm R},\sigma^2(R,z)] = f_{\rm PS}[\delta_{\rm c}-\bar{\delta}_{\rm R},\sigma^2(R_{\rm M},z)-\sigma^2(R,z)]. \quad (4)$$

In this work, we favor a hybrid approach for the biased halo mass function shown in Barkana & Loeb (2004) which adjusts the Sheth-Tormen formula with a relative correction based on the extended Press-Schechter model (see also Yu & Lu 2005)

$$f_{\rm bias}[\delta_{\rm c},\sigma^2(R_{\rm M},z);\bar{\delta}_{\rm R},\sigma^2(R,z)] = f_{\rm ST}[\delta_{\rm c},\sigma^2(R_{\rm M},z)] \times\frac{f_{\rm bias-PS}[\delta_{\rm c},\sigma^2(R_{\rm M},z);\bar{\delta}_{\rm R},\sigma^2(R,z)]}{f_{\rm PS}[\delta_{\rm c},\sigma^2(R_{\rm M},z)]}. \quad (5)$$

2.2 Quasar Emissivity at the Lyman Limit

In some ways, the ionizing emissivity from high-redshift quasars is fully determined by the slope and evolution of the luminosity function which is basically a statistical measure of the joint distribution of quasars in luminosity and redshift. Associated with hundreds of quasar samples during $0\lesssim z\lesssim 6.3$, several theoretical or empirical descriptions of the luminosity function have been proposed in the past. Pei (1995) and Meiksin (2005) provided the standard double power-law luminosity function in good agreement with the observed faint and bright end slopes at $z\leqslant 3$. Haiman & Loeb (1998) discussed an approximate prescription on the basis of the Press-Schechter (1974) mass function while not taking into

account the biasing effects from overdensities. Conversely, Wyithe & Loeb (2002) estimated the luminosity function over a wide range of redshifts using the galaxy merger rates calculated by the excursion set formalism of Bond et al. (1991) and Lacey & Cole (1993). Nevertheless, since the collapsed objects are rare at high redshifts, the merger probability is actually low, and then the merger rates should be smaller than the halo formation rates. Following this consideration, we reexamine the quasar luminosity function under the hypothesis that the quasar emission is triggered by the halo formation beyond $z \sim 2$. Furthermore, we emphasise the overdense environment where quasars reside and therefore prefer the hybrid mass function of dark matter halos in our representation. Similar to the framework described in Haiman & Loeb (1998), we write the improved quasar luminosity function, defined as the comoving number density of quasars having rest frame B-band luminosities between L_B and $L_B + \Delta L_B$ at redshift z, as

$$\Phi(L_B, z) \approx \frac{t_{\rm dc,0}}{H_0^{-1}} \sqrt{\frac{\Omega_{\rm m}}{a^5} + \frac{\Omega_\Lambda}{a^2}} \frac{1}{5.7 \times 10^3} \frac{1}{\epsilon} \frac{d^2 n_{\rm bias}}{dM dz} \Big|_{M=\frac{L_B}{5.7\times 10^3 \epsilon}}, \tag{6}$$

where

$$\frac{dn_{\rm bias}}{dM} = \frac{(1+\bar{\delta}_{\rm R})\bar{\rho}}{M} \times \left| \frac{d\sigma^2(R_{\rm M}, z)}{dM} \right| f_{\rm bias}[\delta_{\rm c}, \sigma^2(R_{\rm M}, z); \bar{\delta}_{\rm R}, \sigma^2(R, z)] \tag{7}$$

is the biased halo mass function in the regions with average overdensity $\bar{\delta}_{\rm R}$. We have $\epsilon \equiv M_{\rm bh}/M_{\rm halo}$ to describe the ratio of final black hole mass to halo mass and assume it is the same for all halos, and $t_{\rm dc,0}$ is the e-folding time for the universal light curve (Haiman & Loeb 1998). The best-fit values of these parameters are $\epsilon = 10^{-3.2}$ and $t_{\rm dc,0} = 10^5$.

For our representative model, we calculate the logarithmic slope of the quasar luminosity function in the redshift range $2 \lesssim z \lesssim 6$, and compare it to the existing observational data together with the basic model results (Haiman & Loeb 1998, *dashed line)*. Fortunately, as shown in Figure 1, we find that our simple considerations cause a better fit than the basic model. Actually, one may notice that the developed approach employs a simple expression to achieve a higher precision, especially at $2.5 \lesssim z \lesssim 6$, which is in quantitative agreement with the published measurements.

With respect to the high-redshift quasars, it is commonly believed that all the ionizing photons are released into the IGM, thereby, here, we first assume $f_{\rm esc} = 1$. Next, we integrate the quasar luminosity function so that the comoving ionizing emissivity is in units of $\rm erg\ s^{-1}\ Hz^{-1}\ Mpc^{-3}$ at frequency ν and redshift z

$$\epsilon(\nu, z) = \int_{L_{\rm min}}^{\infty} L_\nu(L_B, \nu) \Phi(L_B, z)\, dL_B, \tag{8}$$

where $L_\nu(L_B, \nu)$ is the luminosity of a quasar with a B-band luminosity L_B at frequency ν. Srbinovsky & Wyithe (2007) argued that the value of the integral depends sensitively on the quasar minimum luminosity $L_{\rm min}$ and gave the best fit value $L_{\rm min} = 10^{12.5} L_{B,\odot}$, which is consistent with the magnitude observed in SDSS (Fan et al. 2001). A fainter limit $L_{\rm min} = 10^{11.17} L_{B,\odot}$ is suggested by Bolton & Haehnelt (2007c) according to the faintest magnitude detected by combined deep X-ray and optical surveys (Dijkstra & Wyithe 2006; Shankar & Mathur 2007). We have computed this integral with these two lower limits, and both of the resultant quasar ionization rates are plotted in Figure 4 for comparison. Theoretically, contributions to the ionizing background at frequency ν and redshift z would be made by photons emitted at higher redshift z' with higher frequency ν'. Meanwhile, as discussed in detail by Madau, Haardt & Rees (1999), the ionizing photons would experience attenuation as they propagate through the clumpy IGM. We therefore integrate the emissivity over the history of the Universe and give the ionizing flux at frequency ν and redshift z by

$$J(\nu, z) = \frac{c}{4\pi}(1+z)^3 \int_{\infty}^{z} \epsilon(\nu', z') e^{-\tau(z', z)} \frac{dt}{dz'}\, dz', \tag{9}$$

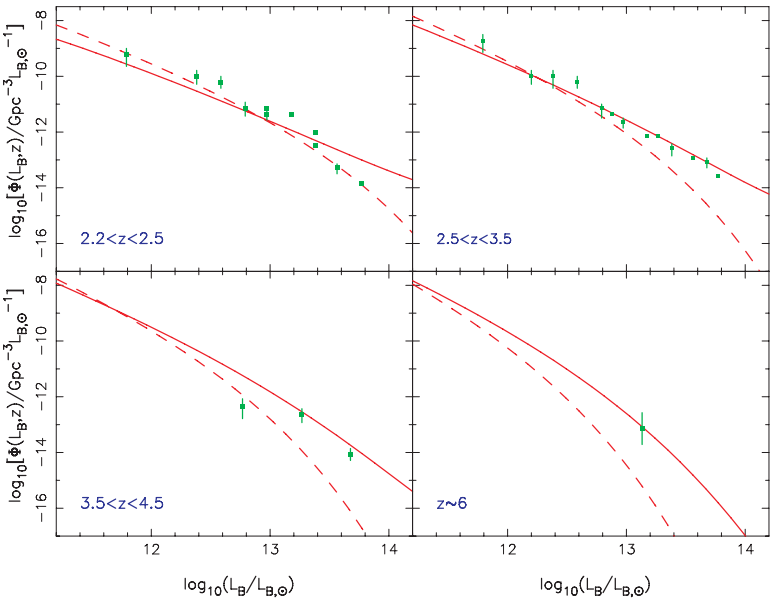

Fig. 1 The observed and model rest frame B-band luminosity function of high-redshift quasars. The data at $z \lesssim 4$ is taken from Pei (1995), and the other points are from Fan et al. (2001). In each panel, the solid line shows our fits based on the hybrid halo mass function. For comparison, the dashed line displays the results obtained by Haiman & Loeb (1998).

in which $\nu' = \nu(1+z')/(1+z)$ and $\tau(z',z) = \int_{z'}^{z} \frac{cdt}{dz} \frac{1}{\lambda_{\rm mfp}(z)}\, dz$ measures the photo-electric absorption in the IGM between z' and z. Here, $\lambda_{\rm mfp}(z)$ is the mean free path of ionizing photons that will be discussed in the next section. Obviously, what we are mainly interested in is the ionizing intensity at 912Å ($\nu_{\rm L}$) for a given redshift. For this reason, the value of ν' should be situated in the frequency interval $3.29 \times 10^{15} < \nu' = \nu_{\rm L}[(1+z')/(1+z)] < 5.94 \times 10^{15}$ Hz. To convert from $L_{\nu'}$ to the B-band luminosity, we adopt the broken power-law spectrum for quasars $L_\nu \propto \nu^{-\alpha_{\rm s}'}$, where $\alpha_{\rm s}'$ is the spectral index at the Lyman limit. We then obtain

$$\eta_{\nu'} = \frac{L_{\nu'}}{L_B} = \frac{L_{\nu'}}{L_{\nu_{\rm L}}} \frac{L_{\nu_{\rm L}}}{L_B} = \eta_{\nu_{\rm L}} \Big(\frac{1+z'}{1+z}\Big)^{-\alpha_{\rm s}'}, \tag{10}$$

where $\eta_{\nu_{\rm L}} = L_{\nu_{\rm L}}/L_B = 10^{18.05}\,{\rm erg\,s^{-1}\,Hz^{-1}}\,L_{B,\odot}^{-1}$ (Schirber & Bullock 2003). Finally, the quasar ionizing flux at the Lyman limit normalized in physical units of $10^{-21}\,{\rm erg\,cm^{-2}\,s^{-1}\,Hz^{-1}\,sr^{-1}}$ can be written as a function of redshift:

$$J_{\rm Q}(z) = 10^{21} \frac{c}{4\pi} (1+z)^3 \times \eta_{\nu_{\rm L}} \int_{\infty}^{z} \frac{dL_B^{\rm tot}(z')}{dV} \Big(\frac{1+z}{1+z'}\Big)^{\alpha_{\rm s}'} e^{-\tau(z',z)} \frac{dt}{dz'}\, dz', \tag{11}$$

where

$$\frac{dL_B^{\rm tot}(z)}{dV} = \int_{L_{\rm min}}^{\infty} L_B \Phi(L_B, z)\, dL_B \tag{12}$$

is the total B-band luminosity per comoving volume.

2.3 Star Emissivity at the Lyman Limit

Since the galaxy luminosity function is always described by several observationally-motivated or parametric models, such as the Schechter form (1976), we cannot estimate the comoving emissivity from galaxies in a similar fashion as the quasar emissivity over a wide range of redshifts. To maintain the density dependence in our theoretical model, we employ the star formation history to derive the comoving density of stellar ionizing photons, and in turn yield the expected ionizing background intensity at the Lyman limit. Here, we adopt the "local source" approximation to account for the photon attenuation in the IGM.

As gas infalls into the dark matter halos, the star formation would be promoted only if the gas cooling due to radiation by atomic, molecular or metal lines can be efficient. Following the arguments presented by many other authors (e.g. Haiman et al. 1996; Somerville et al. 2001; Abel et al. 2002; Springel & Hernquist 2003), the precise cooling induced by molecular and metal transitions would be suppressed and far from clear spanning the redshift range $2 < z < 10$. Furthermore, the atomic cooling is very limited in halos with virial temperatures below $\sim 10^4\,\mathrm{K}$. We therefore consider the star formation efficiency (i.e., the fraction of collapsed matter that forms stars) in halos with $T_{\rm vir} > 10^4\,\mathrm{K}$ at $2 < z < 10$ when the molecular and metal cooling are neglected. Indeed, the key to measuring the star formation history lies in understanding the evolution of normalized star formation rate. We set this formation rate using a general fitting formula represented by Hernquist & Springel (2003) which showed that the feedback due to galactic winds maintains the normalized star formation rate roughly at a constant level for virial temperatures in the range $10^4 - 10^{6.5}\,\mathrm{K}$, and it rises about three times higher for hotter temperatures. Thus, in the rare overdensities, the star formation efficiency can be described as

$$f_\star(z) \simeq \int_\infty^z s_0 q(z) \big[F(> M_4, z) + 2F(> M_{6.5}, z)\big] \frac{dt}{dz}\, dz, \tag{13}$$

where $s_0 q(z)$ is the normalized star formation rate for $10^4 < T_{\rm vir} < 10^{6.5}\,\mathrm{K}$ (Hernquist & Springel 2003), and M_4 corresponds to the mass of a halo with virial temperature $10^4\,\mathrm{K}$. Here, we integrate Equation (5) to obtain the mass fraction of halos with masses higher than M

$$F(> M, z) = \int_{\sigma^2(R_{\rm M}, z)}^\infty f_{\rm bias}[\delta_{\rm c}, \sigma^2(R_{\rm M}, z); \bar{\delta}_{\rm R}, \sigma^2(R, z)]\, d\sigma^2. \tag{14}$$

The evolutions of star formation efficiencies with different mass distributions of dark matter halos are plotted in Figure 2. The history of cosmic star formation inferred from theories as well as simulations peaks at $z \sim 5 - 6$ (Ascasibar et al. 2002; Hernquist & Springel 2003). Thus, the mass fraction of baryons in formed stars would increase significantly following this formation process. Towards lower redshifts, especially at $z \leq 4$, the boosted star formation efficiency is clearly presented in Figure 2. Moreover, the hybrid mass function (*solid line*) constrains the values of $f_\star$ to be $10\% - 15\%$, which is consistent with the product in Wyithe & Loeb (2006). In contrast to the cosmic mean density field (*dashed line* and *dot-dashed line*), one can see that the star formation in the overdense environment (*solid line* and *dotted line*) is indeed enhanced at the same redshift.

We now proceed to determine the star ionizing emissivity (i.e., ionizing photon emission rate per unit comoving volume) using

$$\dot{N}_\star(z) \simeq 4000(1 + \bar{\delta}_{\rm R}) N_{\rm b} f_{\rm esc} \frac{df_\star(z)}{dt}, \tag{15}$$

where we assume that each baryon in the formed stars roughly produces 4000 UV photons (e.g. Barkana & Loeb 2001; Yu & Lu 2005). N_b is the baryon comoving number density in the Universe. Since these ionizing sources generally appear in high-density regions and some fraction of the UV photons should be locally absorbed, we employ the escape fraction $f_{\rm esc}$ to describe this scenario.

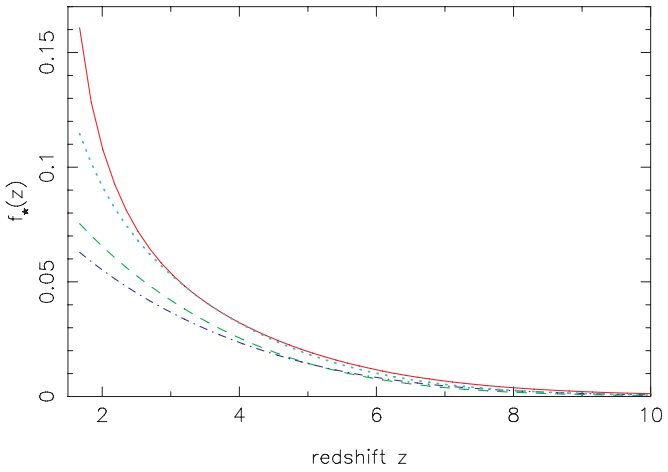

Fig. 2 Star formation efficiency as a function of redshift. Quantitative estimates with four mass functions of dark matter halos are presented. The solid line corresponds to the hybrid model (Barkana & Loeb 2004). The dotted line is predicted by the extended PS theory (Bond et al. 1991), while the dashed line and the dot-dashed line are the approaches based on the Press-Schechter (1974) theory and the Sheth-Tormen (1999) formula, respectively.

Owing to the rapid increase with lookback time of the absorbers, the mean free path of ionizing photons at 912Å would become so small that most of the ionizing photons experience attenuation at high redshifts and the ionizing background radiation turns out to be largely local. In principle, we should use the full integral expression, as described in Equation (9), to calculate this attenuation, but it is also useful to introduce the absorption length, $\Delta l(\nu_{\rm L}) \simeq 33{\rm Mpc}[(1+z)/4]^{-4.5}$, that defines a proper distance only within which the UV emissivity contributes to the ionizing background intensity. Thus, the ionizing flux emitted from the first stars at the Lyman limit can be written as (Madau et al. 1999)

$$J_\star(z) = 10^{21}\frac{1}{4\pi}h\alpha_{\rm s}\dot{N}_\star(z)(1+z)^3\Delta l(\nu_{\rm L}) \tag{16}$$

in physical units of 10^{-21} erg cm^{-2} s^{-1} Hz^{-1} sr^{-1}. Here, h is the Planck constant and $\alpha_{\rm s}$ is the spectral index at $\lambda < 912$Å for galaxies. So far, with an appropriate choice for model parameters, we can give a robust estimate of the ionizing background generated by star-forming galaxies and quasars at a fixed (z, M, R) in the post overlap era of reionization. Furthermore, we emphasis that the mean free path of ionizing photons would play an important role in the prediction of the quasar-governed ionization state at lower redshifts.

2.4 Free Parameters

The free parameters of our reionization model can be summarized as follows:

1. $f_{\rm esc}$: escape fraction of stellar ionizing photons
2. $\alpha_{\rm s}$: Lyman limit spectral index for galaxies
3. $\alpha_{\rm s}'$: Lyman limit spectral index for QSOs
4. $L_{\rm min}$: lower limit of the quasar luminosity

While many empirical measurements and theoretical studies are underway, the escape fraction $f_{\rm esc}$ remains poorly constrained at present. Taking into account most of the existing constraints, Ciardi & Ferrara (2005) concluded that the value of $f_{\rm esc}$ should be $\lesssim 0.15$. The observations of the Lyman-break galaxy population also indicate the escape fraction of $\sim 10\% - 15\%$ (Shapley et al. 2006;

Siana et al. 2007). Nevertheless, Razoumov & Sommer-Larsen (2006) argued that $f_{\rm esc}$ would vary with redshift, and Inoue, Iwata & Deharveng (2006) suggested $f_{\rm esc} > 0.1$ may be appropriate at $z \approx 6$. However, a larger $f_{\rm esc} \gtrsim 0.2$ is required by Bolton & Haehnelt (2007c) in their hydrodynamical simulations of the estimates of photoionization rate at $z = 5$ and 6. Additionally, Gnedin, Kravtsov & Chen (2007) found angular averaged escape fractions of $1\% - 3\%$ over the entire redshift interval $3 < z < 9$, derived from fully self-consistent cosmological simulations which include radiative transfer and resolve the interstellar medium in modest sized galaxies at high redshifts. In our calculation, the fit for escape fraction is therefore performed over the value range $0.01 \leqslant f_{\rm esc} \leqslant 0.2$.

As noted before, the spectral shapes of the ionizing emissivity from high-redshift galaxies and quasars, which should be characterized by direct measurements, also introduce considerable uncertainties. We adopt the galaxy spectral energy distribution based on the synthetic model spectrum of Leitherer et al. (1999) that indicates

$$L_\nu \propto \begin{cases} \nu^0 & (912 < \lambda < 3000\text{Å}); \\ \nu^{-3} & (\lambda < 912\text{Å}), \end{cases}$$

with an additional break at the Lyman limit. However, since the spectral shape depends strongly on star formation history, the presence of Population III stars would harden this energy spectrum with $\alpha_{\rm s} \sim 1$. On the other hand, Madau, Haardt & Rees (1999) analyzed the rest-frame optical and UV spectra of Sargent, Steidel & Boksenberg (1989) together with Francis et al. (1991), and further formalized the quasar spectral energy distribution

$$L_\nu \propto \begin{cases} \nu^{-0.3} & (2500 < \lambda < 4400\ \text{Å}); \\ \nu^{-0.8} & (1050 < \lambda < 2500\ \text{Å}); \\ \nu^{-1.8} & (\lambda < 1050\ \text{Å}), \end{cases}$$

where the different slopes have been continuously matched. Moreover, based on the *Hubble Space Telescope* (HST) EUV observations of radio-quiet quasar spectra at intermediate redshifts, Zheng et al. (1997) pointed out that the fiducial value and uncertainty for $\alpha_{\rm s}'$ should be 1.83 ± 0.15 at $\lambda < 1050$ Å. A somewhat harder slope for quasars with $\alpha_{\rm s}' = 1.57 \pm 0.17$ has been suggested by Telfer et al. (2002) by utilizing the more recent EUV survey from HST in the wavelength range $500 \lesssim \lambda \lesssim 1200$ Å. The values for $L_{\rm min}$ permitted by measurements have been discussed in the previous sub-section.

From Equations (15) and (16), one can see that the ionizing radiation due to star-forming galaxies is proportional to $f_{\rm esc}$ and $\alpha_{\rm s}$ at a given redshift. Meanwhile, it has been clearly shown that smaller values of $L_{\rm min}$ and $\alpha_{\rm s}'$ would induce a higher ionizing emissivity from quasars. In order to determine how the inferred ionizing background intensity scales with these free parameters, we repeat the calculation procedure for many varying choices. Finally, the best fit combination required to reproduce the observations as well as simulations is given by $(f_{\rm esc}, \alpha_{\rm s}, \alpha_{\rm s}', L_{\rm min}) = (0.03, 2, 1.5, 10^{12.5} L_{B,\odot})$ at $z \sim 2 - 6$.

3 IONIZATION STATE OF COSMIC HYDROGEN

As represented above, the mean free path of ionizing photons, which is essentially determined by the critical overdensity for hydrogen ionization $\Delta_{\rm crit}(z)$, is indeed crucial to our reionization model. To begin, the post-overlap evolution of the photon mean free path $\lambda_{\rm mfp}$ is carefully quantified. In addition, we further compare the inferred photoionization rate and the Lyα opacity with the recent observations to draw stronger constraints on the expected $\lambda_{\rm mfp}$.

3.1 Mean Free Path

We employ a simple model described in Miralda-Escudé (2000, hereafter MHR00) to consider how the mean free path fares in the post-overlap phase of reionization. Within this model, it is assumed that at any time, gas at densities $\Delta > \Delta_{\rm crit}$ is still neutral, while gas in a region with lower densities is highly ionized. Here, we set $\Delta \equiv \langle \rho \rangle_{\rm R} / \bar{\rho}$ to describe the inhomogeneous nature of the intergalactic medium. The mean free path is then defined as the typical length of regions with $\Delta < \Delta_{\rm crit}$ along random lines

of sight. In reality, one may notice that the geometrical shape of the local structures would cause some spatial variations in the mean free path. However, once the individual ionized regions have overlapped, the ionizing photons will propagate further through the IGM and hence the corresponding mean free path should equal or even exceed the average separation between ionized bubbles. This indeed reduces the local conditional dependence of the mean free path for ionizing photons. During $2 \lesssim z \lesssim 6$, we therefore adopt the very simple approach

$$\lambda_{\rm mfp} = \lambda_0 (1 - F_{\rm V})^{-2/3}, \tag{17}$$

where $F_{\rm V}$ is the volume-weighted filling factor of HII and we use the scale $\lambda_0 H(z) = 60\ {\rm km\,s^{-1}}$. The filling factor $F_{\rm V}$ addresses the fraction of volume within which all gas at densities below $\Delta_{\rm crit}$ has been ionized at redshift z and can be described as

$$F_{\rm V} = \int_0^{\Delta_{\rm crit}(z)} P_{\rm V}(\Delta)\, d\Delta. \tag{18}$$

The probability density function (PDF) for gas overdensity has been set utilizing a good fit to the hydrodynamical simulations

$$P_{\rm V}(\Delta) d\Delta = A \exp\Big[- \frac{(\Delta^{-2/3} - C_0)^2}{2(2\delta_0/3)^2} \Big] \Delta^{-\beta}\, d\Delta. \tag{19}$$

The fit parameters at $z = 2, 3$ and 4 were listed in Table 1 of MHR00 and an extrapolation was also given at $z = 6$ by assuming $\delta_0 = 7.61/(1+z)$. Nevertheless, some different fits were proposed by other calculations (e.g. Chiu et al. 2003). It has been illustrated that these fit values based on a single simulation with a particular set of cosmological parameters should depend significantly on the background cosmology especially at small scales, and further argued that σ_8 would be an essential ingredient in parameterization for the gas PDF. In the current work, we adopt the fit parameters derived from the simulations of MHR00 as a result of the similar sets of σ_8. To obtain the gas PDF at various redshifts, we simply fit the power law exponent β as a continuous function of redshift with a maximum of $\beta_{\rm max} = 2.5$, and then

$$\beta \approx {\rm Min}[2.5, 2.7 - 1.37/(1+z)]. \tag{20}$$

Within this prescription, we can reproduce the published fits to better than 2.3% at a given redshift. The remaining constants A and C_0 are fixed by demanding that the total volume and mass to be normalized to unity.

In this instance, the mean free path $\lambda_{\rm mfp}$ is directly linked to the critical overdensity $\Delta_{\rm crit}$. It is commonly believed that the value of $\Delta_{\rm crit}$ is fixed prior to overlap, after which it evolves with redshift. For simplicity, $\Delta_{\rm crit}$ is always assumed to be constant in many previous studies (see Wyithe & Loeb 2003; Yu & Lu 2005; Srbinovsky & Wyithe 2007). As a result, the observational data of the mean free path is just recovered roughly by the theoretical curve (as shown in fig. 1 of Srbinovsky & Wyithe 2007). Furthermore, these predicted values would introduce some considerable uncertainties to the subsequent computations. Rather than this, we can do slightly better by tracing the redshift dependence of the critical overdensity in the post-overlap era of reionization. To match the observed flux decrement in QSO absorption spectra (Rauch et al. 1997), the independent measurements of the critical overdensity are contained at $z = 2$, 3 and 4 (MHR00). We then search the appropriate value of $\Delta_{\rm crit}$ at various redshifts by χ^2 minimization fitting, and further extrapolate the prediction to higher redshift. The result is

$$\Delta_{\rm crit}(z) = a \Big(\frac{1+z}{5} \Big)^b + c, \tag{21}$$

where $(a, b, c) = (124.856, -3.623, -32.892)$.

From Figure 3, it appears likely that the critical overdensity for hydrogen ionization $\Delta_{\rm crit}$ rises from 4 at $z = 6$ to 700 at $z = 2$, and exceeds the critical value for collapse (*dotted line*) at $z \sim 3.2$. This strongly suggests that the ionized regions around high-redshift quasars are already virialized and are no longer part of the IGM at low redshifts. Then the mass fraction of neutral hydrogen should be

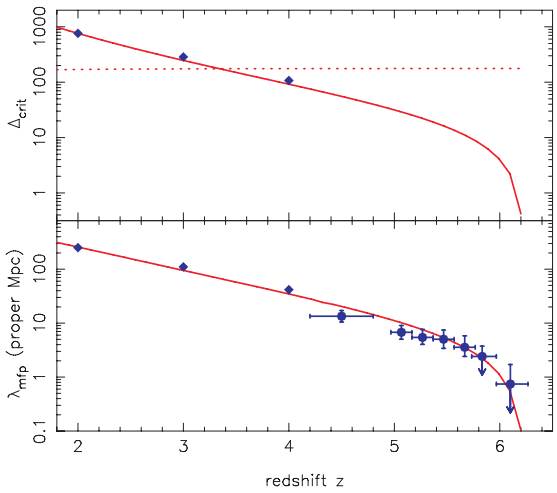

Fig. 3 Evolution of the critical overdensity for hydrogen ionization $\Delta_{\rm crit}(z)$ (*top panel*) and the derived photon mean free path $\lambda_{\rm mfp}$ (*bottom panel*) over the redshift range $2 \lesssim z \lesssim 6$. The corresponding thresholds for collapse are also plotted as the dotted line. Observational data is from MHE00 (diamonds) and Fan et al. (2006, circles). Our theoretical prediction (solid line) agrees quite well with the measurements.

very limited in these overdense regions. Based on the fitted $\Delta_{\rm crit}$, we estimate the mean free path $\lambda_{\rm mfp}$ using Equation (17), and find a similar redshift dependence on the critical overdensity $\Delta_{\rm crit}$. Also note that $\lambda_{\rm mfp}$ evolves much as the reionization front progresses to higher density regions, and the trend becomes mildly sharp at $z \sim 5-6$. The expected increase could be due to two effects: (1) increase in the emissivity of ionizing photons, and (2) increase in the inhomogeneity of the IGM. Approaching $z = 6$, the mean free path is nearly 1 proper Mpc which is comparable to the typical separation between ionizing regions, provided that the mean free path approximately obeys the average correlation scales of clustered galaxies at high redshifts. However, along with the reionization progress, the mean free path of ionizing photons would increase by hundreds of times, to ~ 200 proper Mpc at $z = 2$, which is then controlled by the Lyman-limit systems. Additionally, for higher redshifts, the assumed highly ionized limit in MHR00 turns out to be obviously not true, and Furlanetto, Haiman & Oh (2008) set $\lambda_0 H(z) = 30\ {\rm km\,s^{-1}}$ for corrections. In our reionization model, the volume-weighted filling factor $F_{\rm V}$ reaches unity at $z \simeq 6.2$ which is defined to be the average overlap redshift in the remainder of this paper.

3.2 Photoionization Rate and the Inferred Lyα Optical Depth

Based on the fit values of the mean free path, the quasar ionizing intensity can be calculated from Equation (11), and we now proceed to examine the photoionization rate in the IGM. The derived evolutionary features will provide a sensitive test of the adopted model parameters as well as the predicted photon mean-free-path when compared directly with existing observations and simulations. As before, we have

$$\Gamma = 4\pi \int_{\nu_{\rm L}}^{\infty} \frac{J_\nu}{h\nu} \sigma_\nu \, d\nu, \tag{22}$$

where σ_ν is the HI photoionization cross-section and h is the Planck constant. Similar to many other studies (e.g. Fan et al. 2002; Srbinovsky & Wyithe 2007; Wyithe et al. 2007), we acquire a simple quantitative relation between Γ and $J = J_\star + J_{\rm Q}$,

$$\Gamma_{-12} = 1.72 J_{-21}, \tag{23}$$

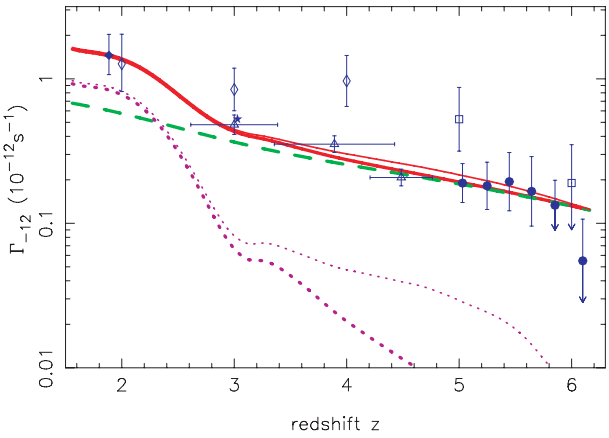

Fig. 4 Comparison of the hydrogen photoionization rate computed from the represented reionization model with the published constraints taken from observations and simulations. The dashed line corresponds to the contribution from star-forming galaxies alone, while the thick dotted line and thin dotted line represent the quasar emissivity calculated with $L_{\rm min} = 10^{12.5} L_{B,\odot}$ and $L_{\rm min} = 10^{11.17} L_{B,\odot}$ respectively. The corresponding combined ionization rates are separately plotted by the thick solid line and thin solid line. The filled diamonds, star and circles are from Tytler et al. (2004), Shapley et al. (2006) and Fan et al. (2006) based on the recent measurements using the Lyα and Lyβ transitions together with the emission from Lyman break galaxies. The open diamonds, triangles and squares are taken from Bolton et al. (2005), McDonald & Miralda-Escudé (2001) and Bolton & Haehnelt (2007c) based on the high-resolution hydrodynamical simulations. The related technical details can be found in the original literature.

in which Γ_{-12} is the ionization rate in units of 10^{-12} s^{-1}, and J_{-21} is the total ionizing flux at the Lyman limit in physical units of 10^{-21} erg cm^{-2} s^{-1} Hz^{-1} sr^{-1}.

Just as we saw in Figure 4, our model prediction for the photoionization rate (*thick solid line*) closely matches the measurements as well as the simulations over the redshift range $2 \lesssim z \lesssim 6$. Here, we adopt the typical halo mass $M = 10^{13} M_{\odot}$ and the comoving sphere radius $R = 5(1+z)\,{\rm Mpc}$ which is centered on the high-redshift quasars. We also carry out similar computations with a likely minimum value for host halo mass $M = 10^{12} M_{\odot}$ (Alvarez & Abel 2007), and find it influences our results by less than 15%. For comparison, the photoionization rates with $L_{\rm min} = 10^{11.17} L_{B,\odot}$ are shown by the *thin dotted line* (quasars only) and the *thin solid line* (quasars and galaxies) separately. One can see that the fainter limit just boosts the combined photoionization rate up to the order of $\sim 10\%$ during $3 < z < 6$. Beyond $z \sim 3$, the first stars dominated the ionization state of cosmic hydrogen. Nevertheless, the quasar emissivity increased rapidly and even exceeded the star-forming galaxies towards lower redshifts. On the other hand, the radiative feedback, especially surrounding high-redshift quasars, actually suppressed this rapid increase around $z = 2$. Notice that the somewhat higher ionization rates, plotted as *open diamonds* and *open squares* in Figure 4, can be interpreted as a result of the different free parameters adopted in Bolton et al. (2005) and Bolton & Haehnelt (2007c), such as $f_{\rm esc} = 0.2$ and $L_{\rm min} = 10^{11.17} L_{B,\odot}$, because a larger escape fraction of the stellar ionizing photons directly causes a higher ionization rate in the IGM that is proportional to $f_{\rm esc}$. Fortunately, our theoretical expectation (*thick solid line*) is nearly consistent with all the measured data points. As first noted by Cen & McDonald (2002) in a small sample of SDSS quasars, we also find that the evolutionary trend seen in Figure 4 turns relatively flat between $z \sim 5$ and 6. This lack of evolution in Γ would be attributed to the short increase in the star formation efficiency at the same redshift range as shown in Figure 2.

Following the similar treatments by other authors, we assume that the IGM is isothermal and photoionized by a uniform UV background, and the GP optical depth therefore depends inversely on the

photoionization rate. For a region of IGM with overdensity Δ

$$\tau(\Delta) \propto \frac{(1+z)^{4.5}(\Omega_{\rm b}h^2)^2\alpha(T)}{h\Gamma(\Delta,z)\Omega_{\rm m}^{0.5}}\Delta^2. \tag{24}$$

On the assumption that the local photoionization and recombination are in equilibrium, one can determine the state equation of the IGM $T(\Delta) = T_0\Delta^\gamma$ with $T_0 \sim 1-2\times10^4\,{\rm K}$ and $\gamma = 0$. Thus, we have

$$\tau(\Delta) = \tau_0\Big(\frac{1+z}{7}\Big)^{4.5}\Big(\frac{0.05}{\Gamma_{-12}(z)}\Big)\Delta^2. \tag{25}$$

We are allowed to examine the GP optical depth in different Lyman transitions with a different proportionality constant τ_0. Fan et al. (2002) have constrained this constant using Lyα absorption and yielded $\tau_0 = 82$. In an inhomogeneous IGM, the definition of the effective optical depth should be introduced, and the corresponding mean transmitted flux ratio can be given by

$$\mathcal{T} = \langle e^{-\tau}\rangle = e^{-\tau_{\rm eff}} = \int_0^\infty e^{-\tau(\Delta)}P_{\rm V}(\Delta)\,d\Delta, \tag{26}$$

which is averaged over the entire IGM density distribution. Clearly, the $\tau_{\rm eff}$ is not equal but smaller than $\langle\tau\rangle$.

Figure 5 shows the evolution of the effective optical depth for the Lyα transition with redshift. Our analytic model presents a reasonable recovery for the observational data during $2.5 \lesssim z \lesssim 6$, which is comparable to the power-law fit obtained from Fan et al. (2006). It appears likely that the Lyα absorption evolves more rapidly with increasing redshift even if the ionizing background almost remains constant (as shown in Fig. 4). Beyond $z \sim 5.8$, the theoretical prediction slightly deviates from the accelerated evolution of the datasets, and this may be due to the fact that the assumed uniform UV background fluctuates more at higher redshifts. However, the fluctuations will not significantly change our conclusions because at present, the redshift interval we are interested in is $z \sim 2-6$ during which the assumption for the uniform UV background is almost valid. In addition, the derived $\tau_{\rm eff}$ is somewhat smaller than the measurement around $z = 2$, resulting from the deviated quasar luminosity function in our model. The appearance of Lyα opacity implies that most regions along the line of sight are optically thick in the IGM approaching $z \sim 6$.

3.3 Neutral Fraction of Cosmic Hydrogen

Finally, we roughly consider the neutral fraction of cosmic hydrogen following the overlap era of reionization. Based on the post-overlap reionization model of MHR00, the volume weighted neutral fraction can be described as

$$\langle f_{\rm HI}\rangle_{\rm V} = 1 + F_{\rm V}\left[\frac{\int_0^{\Delta_{\rm IGM}} f_{\rm HI}(\Delta)P_{\rm V}(\Delta)\,d\Delta}{\int_0^{\Delta_{\rm IGM}} P_{\rm V}(\Delta)\,d\Delta} - 1\right], \tag{27}$$

where $\Delta_{\rm IGM}$ is the maximum overdensity in the IGM and we set $\Delta_{\rm IGM} = 150$ (Fan et al. 2006; Bolton & Haehnelt 2007c). Here, $f_{\rm HI}(\Delta)$ is the residual neutral hydrogen fraction in an ionized region with overdensity Δ

$$f_{\rm HI}(z,\Delta) = \frac{\tau_{\rm eff}(z)H(z)}{\sigma_\alpha c n_{\rm H}(z,\Delta)}, \tag{28}$$

in which $\sigma_\alpha = 4.48\times10^{-18}{\rm cm}^2$ is the scattering cross-section for Lyα photons, and $n_{\rm H}$ is the proper hydrogen number density at a given z and Δ.

It is clearly shown in Equation (27) that the estimate of $\langle f_{\rm HI}\rangle_{\rm V}$ is very sensitive to the exact value of $1 - F_{\rm V}$ which is nearly 1–3 orders of magnitude larger than the fraction term on the right hand side. We therefore consider the influence of the adopted $F_{\rm V}$ on the expected neutral hydrogen fraction in detail. As discussed in Bolton & Haehnelt (2007c), $F_{\rm V}$ is assumed to be unity at $z \le 6$ owing to the

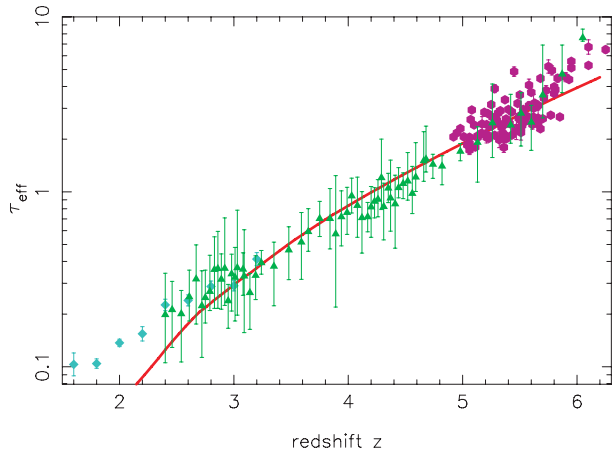

Fig. 5 Lyα effective optical depth as a function of redshift, compared to the observational data with error bars. The best fit evolution computed from our reionization model is shown by the solid line. The filled circles correspond to the combined measurements of $\tau_{\rm eff}$ using the Lyα, Lyβ and Lyγ transitions with conversion factors (Fan et al. 2006). The filled triangles and diamonds give the estimates obtained from Songaila (2004) and Kirkman et al. (2005), respectively, both of which only measure the absorption associated with the Lyα forest.

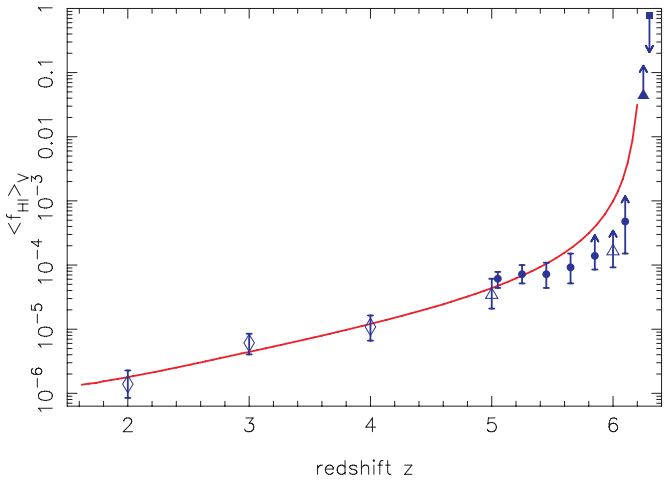

Fig. 6 Redshift dependence of the fraction of volume-weighted neutral hydrogen in the IGM following the overlap of reionization. The solid line gives the theoretical prediction made by our analytic model. Independent observational constraints with error bars at various redshifts are taken from Bolton et al. (2005, open diamonds), Bolton & Haehnelt (2007c, open triangles), Fan et al. (2006, filled circles), Mesinger & Haiman (2007, filled triangle) and Totani et al. (2006, filled square).

highly ionized state in the IGM. In this case, only the fraction term contributes to $\langle f_{\rm HI}\rangle_{\rm V}$, which is of the order $\sim 10^{-5}$ and does not depend strongly on the estimate of mean free path. However, we caution that the value of $F_{\rm V}$ is rather uncertain and quite model-dependent. Although the hydrogen in the IGM is already highly ionized by $z \sim 6$, the $F_{\rm V}$ is likely to be a little smaller than unity, such as $F_{\rm V} = 0.999$, and then $(1 - F_{\rm V})$ becomes the leading term in Equation (27), resulting in a sharp increase in the

estimated neutral fraction. Thus, while the neutral fraction of cosmic hydrogen can in principle provide more stringent constraints on the reionization model, the quantitative estimate of it has no meaning in the post overlap epoch of reionization. Here, we just roughly confirm the strong evolution of the neutral fraction over the redshift range that we probe, and the theoretical prediction for $\langle f_{\rm HI}\rangle_{\rm V}$ is plotted in Figure 6. Around $z = 6$, the estimate dramatically increases by a factor of ~ 3000, to 3×10^{-2}. As we show, the derived $\langle f_{\rm HI}\rangle_{\rm V}$ (*solid line*) is not fully consistent with the published datasets, yet the trend of rapid evolution is clearly established.

4 DISCUSSION

The goal of this work is to characterize the evolution of the ionization state of cosmic hydrogen in the post-overlap phase of reionization. By considering the overdense environment where quasars reside, we present a well-tested reionization model including not only knowledge of IGM properties, but also intrinsic properties of ionizing sources. The structure formation in these overdense regions and consequently the gas distribution, star formation, and reionization of neutral hydrogen are significantly biased away from those in the regions with cosmic mean density. Obviously, the enhanced densities induce higher formation and growth rates for both stars and QSOs, and further affect the ultraviolet emission together with the nature of reionization. Associated with the appropriate combination of free parameters and the robust estimates of photon mean free path, the ionizing background intensity contributed by galaxies and quasars is readily computable from our analytic model. Furthermore, we are able to quantitatively describe the evolutions of photoionization rate, Lyα effective optical depth and neutral hydrogen fraction over the redshift range $2 \lesssim z \lesssim 6$. By comparing our expectations to observed absorption spectra of high-redshift quasars together with hydrodynamical simulations, we provide more stringent constraints on the allowed ranges of free parameters as well as the mean free path for ionizing photons.

Adopting a hybrid expression for the biased mass function of dark matter halos, we improve the quasar luminosity function with the similar framework described in Haiman & Loeb (1998). We investigate the logarithmic slope of this luminosity function in the redshift interval $z \sim 2 - 6$, and find that our simple prescription can offer a better fit to the observations, particularly at $z > 2.5$. For the star formation history, we find that the enhanced densities surrounding high-redshift quasars would introduce an increase in the star formation efficiency on the order of $25\% - 65\%$ during $2 \leqslant z \leqslant 6$, that reaches 0.11 at $z = 2$. In our model, the ionizing radiation from distant sources is significantly degraded by attenuation which is directly related to the mean free path of ionizing photons. While the exact values of the mean free path are model-dependent, the strong evolutionary trend is clearly detected from $z \sim 4$ to 6. Since there are no independent measurements of $\lambda_{\rm mfp}$, we suggest an alternative way to constrain the expected mean free path through matching the observed flux decrement in quasar absorption spectra. Our calculations reveal a very similar evolution of the mean free path to the critical overdensity for hydrogen reionization. The redshift dependence of these critical overdensities are examined carefully, and then the mean free path is straightforward to compute from $\Delta_{\rm crit}$. We show that the $\lambda_{\rm mfp}$ rises from 1 proper Mpc at $z \simeq 6$ to 250 proper Mpc at $z \simeq 2$. Around $z = 6$, the mean free path reaches ~ 1 proper Mpc which is comparable to the correlation length of star-forming galaxies. Also notice that the estimated critical overdensities are severely restricted to the range of $740 - 4$ for $z = 2 - 6$, which are factors of $4 - 0.02$ larger than the corresponding critical threshold for collapse, indicating a rapid overlap process during this redshift range. We have calculated the photoionization rate Γ_{-12} with two different lower limits on quasar luminosity ($L_{\rm min} = 10^{12.5} L_{B,\odot}$ and $L_{\rm min} = 10^{11.17} L_{\rm B,\odot}$), and found that the quasar ionizing radiation computed with $L_{\rm min} = 10^{11.17} L_{B,\odot}$ would exceed the values computed with $L_{\rm min} = 10^{12.5} L_{B,\odot}$ by a factor of $1.2 - 10.7$ during $3 \leqslant z \leqslant 6$. However, towards lower redshifts, the ionizing background is no longer sensitive to the adopted lower limit. Additionally, we show the strong evolution of the neutral hydrogen fraction over the redshift range $2 \lesssim z \lesssim 6$, and the most dramatic evolution appears shortly after $z = 6$. We analyze this increase process in detail and further point out that the quantitative estimates of neutral fraction is very model-dependent and even not reliable in the post overlap epoch.

For our results, a general agreement with existing measurements is achieved, which enhances our confidence in the theoretical calculations. With future wide-field IR surveys and low-frequency radio experiments (such as 21CMA, LOFAR, MWA and SKA), further theoretical modeling will hopefully improve these constraints and complement our knowledge about the formation and evolution of cosmic structures.

Acknowledgements We would like to thank Da-Ming Chen for helpful comments and discussion during the course of this work. We are also grateful to James S. Bolton for kindly providing us with the observational data of Lyα effective optical depth plotted in Figure 5. We also thank Quan Guo for careful reading of the draft manuscript.

References

Abel, T., Bryan, G. L., & Norman, M. L. 2002, Science, 295, 93
Alvarez, M. A., & Abel, T. 2007, MNRAS, 380, L30
Ascasibar, Y., Yepes, G., Gottlöber, S., & Müller, V. 2002, A&A, 387, 396
Bajtlik, S., Duncan, R. C., & Ostriker, J. P. 1988, ApJ, 327, 570
Barkana, R., & Loeb, A. 2001, Phys. Rep., 349, 125
Barkana, R. 2004, MNRAS, 347, 59
Barkana, R., & Loeb, A. 2004, ApJ, 609, 474
Becker, R. H., et al. 2001, AJ, 122, 2850
Becker, G. D., Rauch, M., & Sargent, W. L. W. 2007, MNRAS, 662, 72
Bolton, J. S., Haehnelt, M. G., Viel, M., & Springel, V. 2005, MNRAS, 357, 1178
Bolton, J. S., & Haehnelt, M. G. 2007a, MNRAS, 374, 493
Bolton, J. S., & Haehnelt, M. G. 2007b, MNRAS, 381, 35
Bolton, J. S., & Haehnelt, M. G. 2007c, MNRAS, 382, 325
Bond, J. R., Cole, S., Efstathio, G., & Kaiser, N. 1991, ApJ, 379, 440
Cen, R., & McDonald, P. 2002, ApJ, 570, 457
Cen, R. 2003, ApJ, 597, 13
Chiu, W. A., Fan, X., & Ostriker, J. P. 2003, ApJ, 599, 759
Ciardi, B., & Ferrara, A. 2005, Space Sc. Rev., 116, 625
Dijkstra, M., Haiman, Z., & Loeb, A. 2004, ApJ, 613, 646
Dijkstra, M., & Wyithe, J. S. B. 2006, MNRAS, 372, 1575
Djorgovski, S. G., Castro, S., Stern, D., & Mahabal, A. A. 2001, ApJ, 560, L5
Eke, V. R., Cole, S., & Frenk, C. S. 1996, MNRAS, 282, 263
Fan, X., et al. 2001, AJ, 122, 2833
Fan, X., Narayanan, V. K., Strauss, M. A., et al. 2002, AJ, 123, 1247
Fan, X., Strauss, M. A., Becker, R. H., et al. 2006, AJ, 132, 117
Francis, P. J., Hewett, P. C., Foltz, C. B., Chaffee, F. H., Weymann, R. J., & Morris, S. L. 1991, ApJ, 373, 465
Furlanetto, S. R., Haiman, Z., & Oh, S. P. 2008, astro-ph/0803.3454
Gnedin, N. Y., Kravtsov, A. V., & Chen, H.-W. 2007, astro-ph/0707.0879
Gunn, J. E., & Peterson, B. A. 1965, ApJ, 142, 1633
Haiman, Z., Rees, M. J., & Loeb, A. 1996, ApJ, 476, 458
Haiman, Z., & Loeb, A. 1998, ApJ, 503, 505
Hernquist, L., & Springel, V. 2003, MNRAS, 341, 1253
Inoue, A. K., Iwata, I., & Deharveng, J.-M. 2006, MNRAS, 371, L1
Jenkins, A., Frenk, C. S., White, S. D. M., et al. 2001, MNRAS, 321, 372
Kauffmann, G., & Haehnelt, M. 2000, MNRAS, 318, L35
Kirkman, D., Tytler, D., Suzuki, N., et al. 2005, MNRAS, 360, 1373
Kriss, G. A., Shull, J. M., Oegerle, W., et al. 2001, Science, 293, 1112
Lacey, C., & Cole, S. 1993, MNRAS, 262, 627
Lehnert, M. D., & Bremer, M. 2003, ApJ, 593, 630
Leitherer, C., Schaerer, D., Goldader, J. D., et al. 1999, ApJS, 123, 3

Lidz, A., McQuinn, M., Zaldarriaga, M., Hernquist, L., & Dutta, S. 2007, ApJ, 670, 39
Loeb, A., & Eisenstein, D. J. 1995, ApJ, 448, L17
Madau, P., Haardt, F., & Rees, M. J. 1999, ApJ, 514, 648
Maselli, A., Gallerani, S., Ferrara, A., & Choudhury, T. R. 2007, MNRAS, 376, L34
McDonald, P., & Miralda-Escudé, J. 2001, ApJ, 549, L11
Meiksin, A. 2005, MNRAS, 356, 596
Mesinger, A., & Haiman, Z. 2007, ApJ, 660, 923
Miralda-Escudé, J., Haehnelt, M., & Rees, M. J. 2000, ApJ, 530, 1
Navarro, J. F., Frenk, C. S., & White, S. D. M. 1997, ApJ, 490, 493
Peebles, P. J. E. 1980, The Large-scale Structure of the Universe (Princeton: Princeton University Press)
Pei, Y. C. 1995, ApJ, 438, 623
Press, W. H., & Schechter, P. 1974, ApJ, 187, 425
Rauch, M., Miralda-Escudé, J., Sargent, W. L. W., et al. 1997, ApJ, 489, 7
Razoumov, A. O., & Sommer-Larsen, J. 2006, ApJ, 651, L89
Sargent, W. L. W., Steidel, C. C., & Boksenberg, A. 1989, ApJS, 69, 703
Schechter, P. 1976, ApJ, 203, 279
Schirber, M., & Bullock, J. 2003, ApJ, 584, 110
Shankar, F., & Mathur, S. 2007, ApJ, 660, 1051
Shapley, A. E., Steidel, C. C., Pettini, M., Adelberger, K. L., & Erb, D. K. 2006, ApJ, 651, 688
Sheth, R. K., & Tormen, G. 1999, MNRAS, 308, 119
Sheth, R. K., & Tormen, G. 2002, MNRAS, 329, 61
Siana, B., Teplitz, H. I., Colbert, J., et al. 2007, ApJ, 668, 62
Smette, A., Heap, S. R., Williger, G. M., Tripp, T. M., Jenkins, E. B., & Songaila, A. 2002, ApJ, 564, 542
Somerville, R. S., Primack, J. R., & Faber, S. M. 2001, MNRAS, 320, 504
Songaila, A. 2004, AJ, 127, 2598
Spergel, D. N., et al. 2007, ApJS, 170, 377
Springel, V., & Hernquist, L. 2003, MNRAS, 339, 312
Srbinovsky, J. A., & Wyithe, J. S. B. 2007, MNRAS, 374, 627
Telfer, R. C., Zheng, W. Kriss, G. A., & Davidsen, A. F. 2002, ApJ, 565, 773
Totani, T., Kawai, N., Kosugi, G., Aoki, K., Yamada, T., Iye, M., Ohta, K., & Hattori, T. 2006, PASJ, 58, 485
Tytler, D., Kirkman, D., O'Meara, J. M., et al. 2004, ApJ, 617, 1
White, R. L., Becker, R. H., Fan, X., & Strauss, M. A. 2003, ApJ, 126, 1
Wyithe, J. S. B., & Loeb, A. 2002, ApJ, 581, 886
Wyithe, J. S. B., & Loeb, A. 2003, ApJ, 586, 693
Wyithe, J. S. B., Loeb, A., & Carilli, C. 2005, ApJ, 628, 575
Wyithe, J. S. B., & Loeb, A. 2006, Nature, 441, 322
Wyithe, J. S. B., Bolton, J. S., & Haehnelt, M. G. 2007, astro-ph/0708.1788
Wyithe, J. S. B. 2008, astro-ph/0804.0468
Yu, Q., & Lu, Y. 2005, ApJ, 620, 31
Zheng, W., Kriss, G. A., Telfer, R. C., Grimes, J. P., & Davidsen, A. F. 1997, ApJ, 475, 469